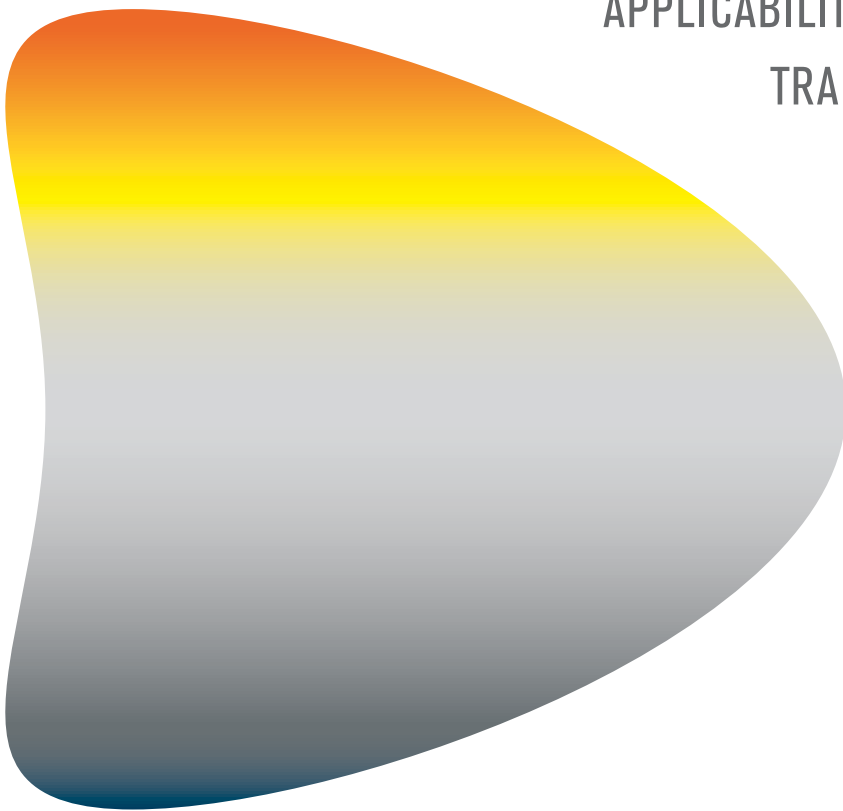

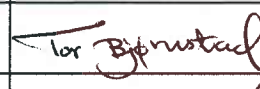



APPLICABILITY AND SENSITIVITY OF GAMMA
TRANSMISSION AND RADIOTRACER
TECHNIQUES FOR MINERAL
SCALING STUDIES



KJELLER Address NO-2027 Kjeller, Norway Telephone +47 63 80 60 00 Telefax +47 63 81 11 68		HALDEN Address NO-1751 Halden, Norway Telephone +47 69 21 22 00 Telefax +47 69 21 22 01		
Report number IFE/KR/E-2006/001			Date 2006-05-02	
Report title and subtitle APPLICABILITY AND SENSITIVITY OF GAMMA TRANSMISSION AND RADIOTRACER TECHNIQUES FOR MINERAL SCALING STUDIES			Number of pages 21 + tables and figures	
Project/Contract no. and name			ISSN 0333-2039	
Client/Sponsor Organisation and reference			ISBN 82-7017-570-6	
Abstract Mineral scaling in petroleum and geothermal production systems creates a substantial problem of flow impairment. It is a priority to develop methods for scale inhibition. To study scaling rates and mechanisms in laboratory flow experiments under simulated reservoir conditions two nuclear methods have been introduced and tested. The first applies the principle of gamma transmission to measure mass increase. Here, we use a 30 MBq source of ^{133}Ba . The other method applies radioactive tracers of one or more of the scaling components. We have used the study of CaCO_3 -precipitation, as an example of the applicability of the method where the main tracer used is $^{47}\text{Ca}^{2+}$. While the first method must be regarded as an indirect method, the latter is a direct method where the reactions of specific components may be studied. Both methods are on-line, continuous and non-destructive, and capable to study scaling of liquids with saturation ratios as low as $\text{SR}=1.5$ or lower. A lower limit of detection for the transmission method in sand-packed columns with otherwise reasonable experimental parameters is < 1 mg CaCO_3 in a 1 cm section of the tube packed with silica sand SiO_2 . A lower limit of detection for the tracer method with reasonable experimental parameters is < 1 μg in the same tube section.				
Keywords: Nuclear techniques, mineral scaling, gamma transmission, radiotracer techniques, oil wells, geothermal wells.				
	Name		Date	Signature
Author(s)	Tor Bjørnstad Emanuel Stamatakis		2006-05-02	
Reviewed by	Tor Bjørnstad		2006-05-02	
Approved by	Tor Bjørnstad		2006-05-02	

Contents	Page
Abstract	1
1 Introduction to mineral scaling	2
2 The main scale components	6
3 The gamma transmission method for scaling studies	7
3.1 Principles	7
3.2 Experimental details	8
3.3 Example of results	10
3.4 Prospects	11
4 The radiotracer (or gamma transmission) method for scaling studies	12
4.1 Principles	12
4.2 Example of results	14
4.3 Prospects	16
5 Conclusions	18
References	20
Tables 1 – 6	
Figures 1 - 15	

**APPLICABILITY AND SENSITIVITY OF GAMMA TRANSMISSION AND
RADIOTRACER TECHNIQUES FOR MINERAL SCALING STUDIES**

TOR BJØRNSTAD

Institute for Energy Technology (IFE), NO-2027 Kjeller, Norway and

University of Oslo, Institute of Chemistry, NO-0135 Oslo, Norway

EMMANUEL STAMATAKIS

Institute for Energy Technology (IFE), NO-2027 Kjeller, Norway and

National Centre for Scientific Research DEMOKRITOS, 15310 Aghia Paraskevi Attikis,

Greece

Abstract:

Mineral scaling in petroleum and geothermal production systems creates a substantial problem of flow impairment. It is a priority to develop methods for scale inhibition. To study scaling rates and mechanisms in laboratory flow experiments under simulated reservoir conditions two nuclear methods have been introduced and tested. The first applies the principle of gamma transmission to measure mass increase. Here, we use a 30 MBq source of ^{133}Ba . The other method applies radioactive tracers of one or more of the scaling components. We have used the study of CaCO_3 -precipitation, as an example of the applicability of the method where the main tracer used is $^{47}\text{Ca}^{2+}$. While the first method must be regarded as an indirect method, the latter is a direct method where the reactions of specific components may be studied. Both methods are on-line, continuous and non-destructive, and capable to study scaling of liquids with saturation ratios as low as $\text{SR}=1.5$ or lower. A lower limit of detection for the transmission method in sand-packed columns with otherwise reasonable experimental parameters is $< 1 \text{ mg CaCO}_3$ in a 1 cm section of the tube packed with silica sand SiO_2 . A lower limit of detection for the tracer method with reasonable experimental parameters is $< 1 \text{ }\mu\text{g}$ in the same tube section.

Keywords: Nuclear techniques, mineral scaling, gamma transmission, radiotracer techniques, oil wells, geothermal wells.

1 Introduction to mineral scaling

Adopting the general definition of P.A. Reed [1] one might say that "scaling is the result of chemical precipitations becoming immobilised in a flowing system". In petroleum and geothermal terminology the "flowing system" is defined by the produced water, gas and oil streams. The chemical components that can precipitate are carried by these streams, and in particular with the waters.

Scaling in petroleum production systems becomes a growing problem in reservoirs where the pressure balance is maintained by injection of waters that are not compatible with the formation waters, and the problem increases as the reservoir grows more mature. In the North Sea the injection water is mainly filtered and deoxygenized seawater. The seawater contains considerable amounts of sulphate (2-3000 ppm) while the formation waters often have a relatively high concentration of heavy alkaline earth metals strontium and barium. See Table 1 for typical analysis of seawater ionic composition and some examples of formation water compositions both from the North Sea and from other parts of the world. Obvious from the examples given is that there may be a large variation in formation water salinity from one reservoir to another, and the relations between concentrations of the dissolved ions may change dramatically. Therefore, contact between injection and formation waters may entail precipitation and scale formation.

For scaling to occur the following conditions must be fulfilled:

- *The saturation index must be positive, i.e. $SI > 0$:*

The stoichiometric solubility product K_{sp} of a compound C_xA_y is defined as

$$K_{sp} = [C^{y+}]^x [A^{x-}]^y \quad (\text{Eqn.1})$$

where $[C^{y+}]$ and $[A^{x-}]$ are the concentrations in mol/l of the cation and anion of the compound, respectively, at saturation. K_{sp} depends on a number of parameters like temperature, pressure, ion strength etc. Accordingly, precipitation requires that the ion

product $[C^{y+}]^x [A^{x-}]^y$ in the perturbed water system (for instance by mixing of two waters with different compositions) $> K_{sp}$ for the existing conditions. Normally, this is expressed as the saturation ratio, $SR > 1$:

$$SR = [C^{y+}]^x \cdot [A^{x-}]^y / K_{sp} > 1 \quad (\text{Eqn.2})$$

Since the saturation index $SI = \log(SR)$ we have that

$$SI = x \cdot \log([C^{y+}]) + y \cdot \log([A^{x-}]) - \log(K_{sp}) > 0 \quad (\text{Eqn.3})$$

When $SI < 0$ the solution is undersaturated while for $SI = 0$ the solution is in equilibrium with the solid phase.

- *There must be adequate conditions for crystal nucleation:*

A certain number of ions of the two kinds must have a chance to come together to start organising in a crystal lattice. These conditions can be met by the existence of various surfaces with appropriate properties in the fluid flow, for instance the reservoir rock itself (scaling in the reservoir), finely suspended particles in the flowing waters or the rough surfaces of pipelines and production equipment in the well and topside. The rate of nucleation is thus dependent upon the degree of supersaturation (saturation index, S) and temperature, which determines the collision frequency against the "catalysing" surface, the surface energy and surface area.

- *Chemical conditions for growth of the nucleated crystal:*

On the microscopic level the change in Gibbs free energy of crystal growth is given by Eqn.4 [9]:

$$d\Delta G/dn = -kT \ln SI + 2\sigma v/r \quad (\text{Eqn.4})$$

where n = the number of molecular units in the particle,

k = Boltzmann's constant

T = temperature

SI = saturation index

σ = particle surface energy

v = molecular volume

r = a measure of particle radius including a shape factor.

Here, $d\Delta G/dn = 0$ at some critical radius $r = r_c$. For nucleated particles with $r < r_c$, $d\Delta G/dn > 0$ which means that the particles are thermodynamically unstable and may totally dissolve again. Accordingly, a necessary condition for further growth is that $r > r_c$ which makes $d\Delta G/dn$ negative, and further growth occurs spontaneously (exothermic reaction).

- *Possibilities and conditions for the crystal to become immobilised in the system:*

For nucleation occurring on stationary rock surfaces, the nuclei may stick to the surface and cause further growth of the nuclei into larger interconnected scale crystals (scale layers) on the rock surface. Such scaling often occurs in the mixing zone close to the wells, and may result in porosity clogging and, hence, seriously reduced permeability. The nuclei formed on rock surfaces may also be mobilized by the flowing liquids and be transported to the well. Here, it may stick to the tubing walls partly by electrostatic attractions, partly by mechanical trapping due to surface roughness. The lingering time on the surface may be sufficiently long for further crystal growth to occur including bridging between the individual crystal. Scaling formed by this mechanism is often relatively porous.

The nucleation and the continuous further crystal growth may also occur directly on the rough tubing surface. The result is often a harder (less porous) scale.

However, many produced waters that have become oversaturated and scale-prone, do not always produce scale. A period of time usually elapses between the achievement of supersaturation and the detectable appearance of formed crystals. This time lag is known as the '*induction time*', t_{ind} .

The induction time may be considered as being made up of several parts. For example, a certain 'relaxation time', t_r , is required for the system to achieve a quasi-state distribution of molecular clusters. Time is also required for the formation of a stable nucleus, t_n , and for the nucleus to grow to a detectable size, t_g (conditions given by Eqn.4). It is very difficult and not practical to obtain measured values of these more theoretical concepts.

In most systems, however, another time lag may be observed. This time lag is known as the 'latent period' and is defined as the onset of a significant change in the system, e.g. the occurrence of massive nucleation or some clear evidence of substantial solution desupersaturation. According to Mullin [10] it may be preferable to record the latent period as the more practical characteristic of the system. Following the definition of Söhnel and Mullin [11], "...the *experimental* induction time (or latent period*) is the time which elapses between the creation of a supersaturation and the first observable change in some physical property of the precipitating (scaling) system, e.g. the appearance of crystals, change in solution conductivity, composition, pH, a change in pressure drop etc".

In this paper we report on gamma transmission and gamma emission (or radiotracer) experiments. Hence, induction time will be taken as the time elapsed from mixing of the two waters until a detectable change has occurred in the gamma attenuation for the transmission technique and in a significant increase in counting rate for the emission technique.

Both nucleation and further crystal growth may be hampered by the use of scale inhibitors. A few examples will be given on the effect of scale inhibitors and how this can be studied in detail with nuclear techniques. However, the subject of scale inhibition will not be treated in detail in the present text.

* Authors' comment

2 The main scale components

The immobilised precipitates of concern in the petroleum and geothermal industry are several. The most abundant during oil production are CaCO_3 , BaSO_4 and SrSO_4 . In addition, SrCO_3 , CaSO_4 , FeCO_3 and $\text{Fe}(\text{OH})_2$ are found in several cases. During gas production, especially when reservoir conditions are acidic due to a substantial content of H_2S , also scales like FeS , ZnS and PbS may be formed. In geothermal fields, the main scale components are carbonates. In many cases the scales formed is a mixture also with corrosion products mainly from steel installations in the production systems. All these scales are rarely pure crystal phases but have mixed compositions. When scale inhibitors are used, the precipitates may even contain a substantial amount of the inhibitor compounds which often are long-chain polymeric acids, leading to a certain reinforcement of the precipitate and increased difficulties for chemical removal.

The scales may form and be accumulated in:

- the near-well rock formation leading to plugging of the pore network and thereby reduced production,
- the well tubing and can, in serious cases, lead to total blocking,
- on surfaces or as sludges in valves, pumps, separators and storage tanks.

The main scale components resulting from mixing of incompatible waters (i.e. injection water and formation water) are the sulphate compounds. The carbonates are mainly formed during depressurization of the fluid system whereby carbon dioxide is released to the gas phase. This causes CaCO_3 to precipitate according to the equation:



While the sulphate scales are most frequently formed close to the perforations and in the lower part of the production tubing, the carbonate scales are mainly formed in the upper

part of the tubing. However, this picture may be complicated by the varying use of reservoir and well chemicals (for instance scale inhibitors).

Table 2 lists the solubility products of the main scale components in pure water at STP conditions.

It is a main priority at oil production companies and geothermal energy producers to combat the scale formation that is responsible for substantial economic losses each year. Thus, intimate knowledge of scale mechanisms and rates at varying conditions is needed for this purpose.

3 The gamma transmission method for scaling studies

3.1. Principles

SR-values in the range $1.5 < SR < 20$ are of interest in geothermal and oil fields. In order to study scaling at low SR-values, down to $SR = 1.5$, a method based on *gamma transmission* measurements has been proposed and tested. This is a relatively simple method to implement in on-line experiments. The following text outlines this method in more detail and presents a few preliminary data on its use.

The gamma transmission method is a non-destructive non-intrusive method to measure mass density in an object by detecting the attenuation of gamma radiation from an external gamma source as it penetrates the object. The principle of this method is illustrated in Fig. 1. Transmission of a mono-energetic beam of collimated photons through a simple absorption sample can be described by Lambert-Beer's equation

$$I = I_0 \cdot e^{-\mu \cdot x} \quad (\text{Eqn.5})$$

where I_0 is the beam intensity before transmission, I_x the beam intensity after transmission, μ the *linear mass absorption coefficient* of the absorbing material with dimension ℓ^{-1} (cm^{-1}) and

x the material thickness (cm). When the sample is composed of several materials, say A, B and C, each with their own mass absorption coefficient and thickness, exponents are additive and the formula becomes

$$I_{ABC} = I_{0,ABC} \cdot e^{-(\mu_A x_A + \mu_B x_B + \mu_C x_C)} \quad (\text{Eqn.6})$$

The linear absorption coefficient for various materials may be found tabulated in the literature, but more general and frequent is the tabulation and use of the *mass absorption coefficient* μ/ρ with dimension cm^2/g . Here, ρ is the material density (g/cm^3). Let us call this parameter μ_m . Introducing this parameter into (Eqn.6) gives:

$$I_{ABC} = I_{0,ABC} \cdot e^{-(\mu_{m,A} x_{m,A} + \mu_{m,B} x_{m,B} + \mu_{m,C} x_{m,C})} \quad (\text{Eqn.7})$$

Here, x_m is the so-called mass thickness with dimension g/cm^2 . The relation between the linear thickness and the mass thickness is simply $x_m = x \cdot \rho$.

Mass absorption coefficients for various elements (or compounds) vary with the gamma energy as illustrated in Fig.2 below. Here, examples of mass absorption coefficients for chemical elements and compounds of primary interest in the present experiments are illustrated (reproduced from [12])

3.2. Experimental details

Fig.3 shows the schematic diagram of the experimental apparatus, which was partly designed and constructed for this study. Twin HPLC pumps drive two solutions, one containing scale forming cations (Ca^{2+}) and the other anions (HCO_3^-). The solutions are pumped through two pre-heating tubes, which raise the solution temperature to the desired test temperature prior to arriving at the mixing point. The combined solution, which now has an $\text{SR} > 1$, passes through our test section (1m long tube of aluminium 6061 with 1cm ID and

a wall thickness of 1 mm) and scale crystals nucleate and grow on its internal surface. The temperature is maintained constant by a heating wire fixed along the tube. To monitor the forming scale, a collimated beam of gamma rays from an appropriately lead-shielded radioactive source of ^{133}Ba is directed through the tube. Since ^{133}Ba emits a number of gamma ray energies with varying intensity and since the highest intensity gamma ray has energy at 356 keV, we have electronically discriminated all energies below about 300 keV. In this way we can, with a reasonable approximation, consider the beam as mono-energetic. The gentle slope of the mass absorption coefficient variation with energy around 300 keV of the elements included in Fig.2 further supports the safe use of this procedure.

Variations in the transmitted intensity recorded by a radiation detector positioned on the opposite side of the tube can then be related to the variations in the mass per unit area of the intervening deposited material (see Fig. 4). To obtain the final profile along the tube axis of the deposits, the tube is moved (scanned) across the stationary source and detector pair. The square collimator opening at the 2x2" NaI(Tl)-detector is 4.5x4.5 mm. Measurements of Ca-content and pH in the exit liquid have been performed at the end of each run on samples collected at certain intervals during the run. For this particular experimental setup, Eqn.7 becomes:

$$I_{x_m} = I_0 \cdot e^{-(2\mu_{m,\text{Al}}x_{m,\text{Al}} + 2\mu_{m,\text{CaCO}_3}x_{m,\text{CaCO}_3} + \mu_{m,\ell}x_{m,\ell})} \quad (\text{Eqn.8})$$

In case of CaCO_3 -scaling on the inner walls of an aluminum tube, the only unknown parameters are x_{m,CaCO_3} and $x_{m,\ell}$. The contribution of the liquid thickness can be corrected for by calibrating the system by removing the liquid (mass absorption of pure air can be neglected relative to CaCO_3) prior to the final measurements after stop of the run. Thus, x_{m,CaCO_3} can be uniquely determined by solving this parameter from Eqn.8:

$$X_{m, \text{CaCO}_3} = \frac{\ln I_0 - \ln I_{x_m} - 2\mu_{m, \text{Al}} \cdot X_{m, \text{Al}} - \mu_{m, \ell} \cdot X_{m, \ell}}{2\mu_{m, \text{CaCO}_3}} \quad (\text{Eqn.9})$$

To keep the experimental work as simple as possible, no gas phase is present in the system. For that reason, the two scaling solutions have been modified so that after mixing them at 1:1 ratio we will obtain a pre-selected saturation ratio as determined by the computer program MultiScale [13].

The choice of aluminum 6061 for the test tube in our experimental system was based mainly on two reasons; its low density (2.70 g/cm^3) compared to other materials such as steel and iron, and its acceptable behavior to corrosion in saline waters especially in absence of H_2S [14]. Generally, the lower the density the more transparent the material is to the γ -rays and, therefore, the higher the accuracy for the measurements of the scale thickness with the implemented technique.

Care has been taken in the mixing process of the two liquids so as to prevent, as far as possible, the creation of regions with higher saturation ratios than selected for the experiments.

3.3. Example of results

Examples of primary gamma attenuation results for the geothermal study of CaCO_3 precipitation at the relatively high $\text{SR} = 20$, a temperature of $185 \text{ }^\circ\text{C}$ and a pressure of 10 bar are given in Fig.4 [15]. In addition, the figure shows the effect of the inhibitor Na_2AMP (amino methylene phosphonic acid disodium salt) added in various concentrations. These experiments were all conducted in tubes without any substrate or preformed scale layer on the tube walls.

The primary data from Fig.4 is converted into reaction rates in Fig.5 by using Eqn. 9. This is data accumulated at a certain distance, 10 cm along the column axis from the mixing

point.

In oilfield studies, one needs to study scaling tendency at considerably lower supersaturation. Fig.6 shows the first gamma attenuation results for the very low saturation ratio of $SR = 1.5$. In Fig.7 the data in Fig.6 is converted into a scaling rate curve. It is obvious that scale formation has been detected at the inlet of the tube after pumping for some hours.

One should bear in mind that the transmission method is a relative method, i.e. it does not directly measure the behaviour of the different components involved but only a change in mass density. For simple scaling systems like for instance $Ca^{2+} + HCO_3^-$ or $Ba^{2+} + SO_4^{2-}$ this is sufficient. However, for mixed scaling with several chemical components involved, the situation becomes more difficult. For unambiguous experiment evaluation one should combine this method either with the radiotracer technique (described below) or with a destructive chemical analytical methods at the end of the experiment.

3.4. Prospects

In order to mimic the situation in the near-well zone, experiments should be conducted with the tube filled with a porous material. This material can for instance be silicate sand. The main question was now how much the increased mass thickness of the sand would affect the sensitivity of the method, i.e. how thin scale layer can be detected with the presently described method. These experiments have not yet started, but we have performed an evaluation of the potential using $CaCO_3$ as an example. This is detailed elsewhere [16]. The conclusion is as follows:

Based on the criteria:

- Unchanged source type (^{133}Ba) and strength (~ 100 MBq)
- Collimator opening of 4.5×4.5 mm
- Counting time of 600 s per point along the tube axis during scans

- A porosity of 40 % in the sand pack, i.e. 60 % is silicate sand

the minimum detection limit will be ~ 100 μm total thickness of CaCO_3 corresponding to a precipitation of about 2 mg in a 1 cm long section of the tube.

Changing the collimator opening to $\text{hxl} = 4.5 \times 25$ mm, thus reducing the spatial resolution of the scale profile along the tube axis, the detection limit is reduced to 30 μm thickness of CaCO_3 which corresponds to about 0.7 mg precipitate in a 1 cm section of the tube. Further increase in sensitivity can be obtained by removing the remaining liquid before scanning, thereby reducing the total "background" mass thickness.

4 The radiotracer (or gamma transmission) method for scaling studies

4.1. Principles

The use of, preferably, gamma-emitting radiotracers for the various components involved in the mineral scaling, constitutes a direct monitoring method where the various components can be followed non-destructively by external gamma detectors. This method has been introduced and studied during the last few years, and thorough descriptions of principles and a selection of various experiments are given in ref.s [17]-[20].

In the following the potential of the method is demonstrated by referring to studies of CaCO_3 precipitation.

Until recently this method has been used only at higher saturation ratios ($\text{SR} \geq 20$), and the reason is briefly described in the text below. The basis of this method is to label the calcium-containing liquid with the radioactive gamma emitter ^{47}Ca (in the chemical form of Ca^{2+}). The radioactive $^{47}\text{Ca}^{2+}$ behaves chemically identical to non-radioactive calcium. When calcium carbonate precipitates, ^{47}Ca will be a messenger for where the precipitation takes place and to what degree (amount of precipitate). The gamma radiation from ^{47}Ca will penetrate the packed bed and be detected by external detectors. In this way, the emission

technique is an on-line non-intrusive and continuous experimental technique.

The experimental setup is illustrated in Fig.7. In the basic setup it is similar to that described for the transmission technique. The differences are the following:

- Several NaI(Tl) γ -detectors may be used simultaneously for the on-line measurements of ^{47}Ca activity. One will be mounted at a fixed position (position 'zero' of the sand-pack), dedicated to measure accurately the induction time. Another may be mounted at the sand-pack exit to measure remaining (non-precipitated) Ca in the exit liquid, while an optional third detector may be mounted somewhere in between. Another detector is used to scan axially the growth of the calcite deposition in the sand-pack during the experiment (γ -scanner).
- The cationic and anionic fluids are prepared into separate piston cylinders mounted in a heating cabinet. In the cationic liquid, the $^{47}\text{Ca}^{2+}$ tracer is mixed. The two separate pumps operate only with water on the bottom side of the pistons.
- A pH-meter is mounted on the high-pressure side of the BPR to monitor changes in the pH in the exit liquid during the experiment.

Solution temperature T_s , differential pressure Δp , pH, absolute system pressure p and $^{47}\text{Ca}^{2+}$ activity (counting rate R) from the various on-line detectors will be logged by computer during the experiment.

Samples are also collected automatically and periodically at the exit end of the sand pack and the activity of ^{47}Ca in solution determined with an off-line high-resolution HpGe detector system. The main gamma energy of ^{47}Ca is 1297 keV. However, by including also its Compton background and lower energies in the counting window, the sensitivity in the experiment may be increased. It is necessary to avoid contribution from ^{47}Sc , which is the daughter nuclide in the decay of ^{47}Ca . The energy window for the detectors is therefore chosen from 350 keV and upwards to avoid the 159 keV γ -quanta from ^{47}Sc .

^{47}Ca has a half-life of 4.54 days, and has to be produced by thermal neutron irradiation of CaCO_3 in IFE's nuclear reactor JEEP II just prior to the experiments. The useful thermal flux is about 10^{13} n/cm²s, the reaction is $^{46}\text{Ca}(n,\gamma)^{47}\text{Ca}$ and the disintegration rate is calculated by Eqn.10:

$$D_{\gamma} = \sigma \cdot \phi \cdot \frac{W}{M} \cdot N_A \cdot I_N \cdot I_{\gamma} \cdot (1 - e^{-\lambda \cdot t_i}) \cdot e^{-\lambda \cdot t_d} \quad (\text{Eqn.10})$$

where

- σ = reaction cross section (10^{-24} cm²)
- ϕ = neutron flux (n/cm²s)
- w = weight of Ca in the irradiated target (g)
- M = atomic weight of natural Ca (g)
- N_A = Avogadro's number
- I_N = natural abundance of the Ca target isotope (fraction)
- I_{γ} = gamma branch (fraction of total disintegrations) within the counting window of interest
- λ = the decay constant $\ln 2/T_{1/2}$ where $T_{1/2}$ is the half-life of the produced radionuclide of interest
- t_i = irradiation time
- t_d = decay time from stop irradiation to start experiment

Natural calcium contains only 0.004% of the target nuclide ^{46}Ca , so there is a limit to how low SR-values that can be studied with natural calcium due to an upper limit to the obtainable specific activity of ^{47}Ca . SR-values in the range 216-20 have been studied with natural calcium as target material

4.2. Example of results

For illustration purposes a few results are given below for an experiment with the

variable parameters given in Table 3. The scaling rate recorded by the fixed detector at the fluid mixing position at the entrance of the packed column is displayed in Fig.8 together with the simultaneously recorded differential pressure across the sand pack. One observes that the induction times recorded by the two methods, represented by the vertical dashed lines, differ enormously. Fig.9 compares the tracer method with the simultaneously recorded pH variations. Here, one observes that the induction times are practically identical within experimental uncertainty. The actual measured induction time values are ~ 9 min for the radiotracer method, ~ 8 min for the pH method and 85-90 min for the Δp method. In similar experiments with different temperatures, saturation ratios, flow-rates and packing material, the large difference is maintained between the γ and the Δp methods while the difference also increases between the γ and the pH methods for lower SR-values, i.e. the pH method records considerably longer induction times.

Fig.10 illustrates the recording of the scanner detector along the sand pack. Through a calibration procedure, these position-specific count rates may be converted into mg of precipitated CaCO_3 . Each individual data point is given here to illustrate the scatter in the recorded count rates corrected for differences in porosity along the axis (as illustrated with the straight horizontal dotted background line). As expected, most of the precipitation takes place in the entrance to the column and decreases with some exponential function towards the end of the tube.

The kinds of data presented above are important for developing and calibrating a reliable scale formation simulation model. Such a model will be used to predict scaling potential and support scale inhibition operations for instance by optimizing near-well scale squeeze treatments.

4.3. Prospects

So far, the applicability of the radiotracer method has been proven and exemplified for CaCO₃ scaling with the use of ⁴⁷Ca²⁺ as a γ -emitting tracer. What are the potential for the study of other types of scale mentioned in Chapter 2? Table 4 lists both γ -emitting tracers and β -emitting tracers for other major and potentially scale-forming components. The former are useful in experiments similar to those described for ⁴⁷Ca²⁺. The latter are applicable for analyzing the exit fluid from the column and when the column at the end of the experiment is subject to sectioning and destructive analysis.

Preferably, the tracers should be produced upon need by thermal neutron irradiation of appropriate target materials. Figs 11-15 illustrates the irradiation yields for potential radiotracers of Ca, Sr, Ba, Fe and Zn using a thermal flux of 10¹³ n/cm²·s and target material of natural elemental compositions. It is possible to improve the yield by the use of isotopically enriched target material. This gives possibility for increasing both the total activity and the specific activity. Some of the more longer-lived ones (like ⁵⁵Fe, ⁶⁵Zn and ¹³³Ba) may be available commercially even under carrier-free, or near carrier-free conditions. Thus, ultra-low SR values (close to 1) can be studied.

For the mentioned CaCO₃ experiments, SR-values lower than ~ 20 cannot be performed by application of natural calcium as target material which contains only 0.004 % of the target nuclide ⁴⁶Ca. SR-values in the order of 1.5 and slightly above can only be reached by applying calcium isotopically enriched in ⁴⁶Ca. This possibility has recently become available to the present authors, and experiments are now under way.

The isotopic abundance of ⁴⁶Ca in the mentioned enriched material is 4.1 %, a thousand-fold increase relative to natural abundance. The potential in applying this material may be seen by estimating the achievable sensitivity at a saturation ratio of SR = 1.5. This exercise is briefly reported below.

Table 5 shows an estimation procedure for the achievable activity concentration obtainable with reasonable use of the expensive isotopically enriched target material. The calculations are based the parameters values given in the table. Using an irradiation time of one half-life (4.54 d), the activity concentration (measured as the number of γ -quanta emitted with energy of 1297 keV) in a 1 L mother solution is calculated to be $D_\gamma = 9.36 \cdot 10^6$ Bq/L. This is already higher activity than used in the previously described experiment with considerably higher RS-values.

Based on this calculation, estimation can be made of the sensitivity of the method. By this expression one understands the lower limit of CaCO_3 precipitate that can unambiguously be detected using the isotopically enriched CaCO_3 -material. Sensitivity calculations are presented in Table 6. In summary, this shows that:

- For a narrow detector collimator with total counting efficiency of 0.1%, a tracer solution produced with 1 half-life irradiation time and a counting time per point of 60 s, 1 ppm CaCO_3 relative to the SiO_2 packing material is unambiguously detected with a relative standard deviation of 19 %.
- Likewise, for a narrow collimator and otherwise identical parameter values, 10 ppm is well detected with a relative standard deviation of 5 %.
- For a wide collimator, a total counting efficiency of 1% and otherwise identical parameter values, 1 ppm CaCO_3 is well detected with a relative standard deviation of 6 %.
- Likewise, for a wide collimator and otherwise identical parameter values, 10 ppm CaCO_3 is very well detected with a relative standard deviation of 1.5 %.

It is possible to improve the sensitivity further at the end of the experiment, in the final axial scan, by removing the remaining tracer-containing liquid before counting. At this stage it is also possible to increase the counting time per point. When doing so, examples of

obtainable sensitivities are:

- For narrow collimation, a total counting efficiency of 0.1 % and a counting time of 600 s per point, 1ppm CaCO₃ is very well detected with a relative standard deviation of 3.2 %.
- Likewise, for narrow collimation, a counting time of 3600 s per point and otherwise identical parameter values, 10 ppm CaCO₃ is very well detected with a relative standard deviation of 0.4 %.
- For wide collimation, a total counting efficiency of 1 % and a counting time of 60 s per point, 10 ppm CaCO₃ is very well detected with a relative standard deviation of 3.2 %.
- Likewise, for wide collimation, a counting time of 600 s per point and otherwise identical parameter values, 10 ppm CaCO₃ is very well detected with a relative standard deviation of 0.3 %.

Further sensitivity is achieved by increasing the irradiation time to two half-lives (~ 9 d). This will result in 50 % more activity of ⁴⁷Ca and imply lower detection limits.

The calculations presented here must be regarded as approximate rather than exact. The results, however, clearly demonstrate the rather high sensitivity of this method. It is a factor of > 1000 more sensitive than the transmission method if everything operates normal. The downside is that the emission method is more work-intensive and resource demanding. However, this method can generate data on scaling rates and concentrations that is outside reach of any other known method.

5 Conclusions

In conclusion, the major achievements during the last few years on the use of nuclear techniques for mineral scaling studies are:

- The introduction and demonstration of the gamma transmission technique for studies of scaling rates and mechanisms in simple on-line laboratory experiments under simulated reservoir conditions (except from pressure). The use of the technique should be limited to relatively simple precipitation reactions where, preferably, only one compound is involved (for instance CaCO_3 , BaSO_4 etc.).
- An example of the sensitivity achievable with the transmission technique is: Lower detection limit of CaCO_3 in the 1 cm ID Al-tube filled with quartz sand is estimated to ~ 0.7 mg in a 1 cm long section of the tube.
- The introduction and demonstration of the radiotracer technology (or emission technique) for the first time in scaling experiments in porous media. This is a direct monitoring technique since it directly follows the precipitating atoms, and may be used to study mixed and complicated mineral scaling where several compounds are involved simultaneously.
- The achievable sensitivity with the radiotracer technique is dependent on the specific activity obtainable for the tracer in question and also on the "background" radiation of unprecipitated radiotracer in the flooding liquid. Using CaCO_3 as an example again, and $^{47}\text{Ca}^{2+}$ as a tracer, detection limits < 1 μg CaCO_3 can be obtained per 1 cm tube section filled with silicate sand.
- Both techniques produce induction times for CaCO_3 scaling which are shorter than the monitoring of the pressure drop (which is a relative technique) as would be expected. For high SR-values similar induction times were obtained with the pH-monitoring (which is also a relative technique). However, for low SR-values the induction times measured with the radiotracer are shorter than that those measured with the pH-electrode. Especially at low bicarbonate concentrations the pH technique becomes uncertain and unreliable.

Financial support from the European Commission, the Norwegian Research Council and the oil company Statoil is gratefully acknowledged.

References

- [1] Reed, P.A.: *in Proc. NIF Symp. Oil Field Chem., Fagernes, Norway, March 9-11, 1987.*
- [2] Oddo J.E. and Tomson M.B.: *Oil & Gas Journal*, **Jan.3**, (1994) 33-37.
- [3] Poggesi G., Hurtevent C. and Brazy J.L.: Technical Paper SPE 68310, *in Proc. 3rd Int SPE Symp. on Oilfield Scale, Aberdeen, UK, 30-31 Jan. 30-31, 2001.*
- [4] Knapstad B.: *in Proc. IBC/AEA Symp. on Advances in Solving Oilfield Scaling. Aberdeen, UK, Nov. 20-21, 1995*
- [5] Street E.H., Jr., Oddo J.E. and Tomson M.B.: *J. Petr. Technol.*, **Oct.**, (1989) 1080-1086
- [6] Bezerra M.C.M., Do Rosario F.F. and Khalil C.N.: *in Proc. IBC/AEA Symp. on Advances in Solving Oilfield Scaling, Aberdeen, UK, Nov. 20-21, 1995*
- [7] Roque C., Marrast J. and Messaoudene N.: *in Proc. NIF Symp. on Oil Field Chem., Geilo, Norway, March 11-13, 1991*
- [8] Collins I.R.: *in Proc. SPE Symp. on Oilfield Scale – Field Applications and Novel Solutions, Aberdeen, UK, Jan. 27-28, 1999*
- [9] Pritchard A.M., Buckley L.C., Smart N.R. and Webb P.J.C.: *in Proc. Oil Field Chem., Geilo, Norway, March 19-21, 1990.*
- [10] Mullin J.W.: *Crystallization.*, 4th edition, Butterworth-Heinemann (2001) 206-210.
- [11] Söhnel O. and Mullin J.W.: *J. of Crystal Growth*, **60** (1982) 239-250
- [12] Hubbell J.H. and Selzer S.M.: Tables of X-Ray Mass Attenuation Coefficients and Mass Energy-Absorption Coefficients, NIST Standard Reference Database 126 July

- 2004.
- [13] MultiScale, Petrotech ASA: <http://www.petronett.com/multiscale/>
- [14] Burda P. A., Chhatre R. M., Nekoksa G. and Hanck J. A.: *in Proc. Internat. Symp. on Solving Corrosion and Problems in Geothermal Systems*, January 17-20, 1983, San Francisco, California.
- [15] Stamatakis E., Müller J. and Chatzichristos C.: Research Report IFE/KR/F-2005/002, 23 pp.
- [16] Bjørnstad T. and Stamatakis E.: *in Proc. 17th Int. Symp. on Oil Field Chemistry*, March 19-22, 2006, Geilo, NORWAY
- [17] Stamatakis E., Haugan A., Chatzichristos C., Stubos A., Muller J. and Dugstad Ø.: Technical Paper SPE 87436, *in Proc. 6th International Symposium on Oilfield Scale*, Aberdeen, UK, May 26-27, 2004.
- [18] Stamatakis E., Haugan A., Dugstad Ø., Muller J., Chatzichristos C., Bjørnstad T. and Palyvos I.: *Chem. Eng. Sci.*, **60**, (2005) 1363-1370.
- [19] Stamatakis E., Stubos A., Palyvos J., Chatzichristos C. and Muller J.: *J. Colloid and Interphase Sci.*, **286**, (2005) 7-13.
- [20] Stamatakis E., Haugan A., Chatzichristos C., Stubos A., Muller J., Dugstad Ø. And Palyvos, I.: *SPE Production & Operations*, **Feb.**, (2006) 33-39.

Table 1. Concentrations of the main ionic components in sea water and a few formation waters.

Ions	Sea water mg/L ^{a)}	Formation waters, concentrations in mg/L									
		I ^{b)}	II ^{c)}	III ^{d)}	IV ^{e)}	V ^{f)}	VI ^{g)}	VII ^{h)}	VIII ⁱ⁾	IX ^{j)}	X ^{k)}
Cations:											
Na ⁺	12.100	9.220	8.440	49.885	19.000	16.800	33.500	39.100	6.300	28.780	65.340
K ⁺	460	164	159	4.468	-	24	554	1.750	330	1.830	5.640
Mg ²⁺	1.130	61	25	915	380	131	374	2.400	330	115	2.325
Ca ²⁺	450	325	150	11.771	2.400	547	2.760	31.000	4.050	1.060	30.185
Sr ²⁺	9	36	44	450	920	-	415	850	90	110	1.085
Ba ²⁺	nd	59	20	15	1.420	6.3	229	900	-	1.050	485
Anions:											
Cl ⁻	20.950	14.409	12.555	99.847	36.800	28.000	59.100	123.895	14.980	47.680	52.360
SO ₄ ²⁻	2.300	nd	14	212	nd	13	14	-	823	nd	nd
HCO ₃ ⁻	170	1.310	1.418	79	600	552	968	110	230	2.090	496

a). Injection sea water Statfjord A, North Sea [1]

b). Formation water Statfjord A, North Sea [1]

c). Formation water Ninian field, North Sea [2]

d). Formation water Block 3, Angola [3]

e). Formation water Njord field, North Sea [4]

f). Formation water East Hitchcock field, DeLee Unit No.1, USA [5]

g). Formation water Namorado field, Campos Basin, Brasil [6]

h). Formation water Tin Fouye Tabankort field, Ordovician zone, Algeria [7]

i). Formation water Tin Fouye Tabankort field, Lias zone, Algeria [7]

j). Formation water Miller field, North Sea [8]

k). Formation water Gyda field, North Sea [8]

Table 2. Stoichiometric solubility products for typical scale minerals.

Compound	Solubility product K_{sp}
CaCO ₃	$3.36 \cdot 10^{-9}$
CaSO ₄	$3.10 \cdot 10^{-7}$
SrSO ₄	$3.44 \cdot 10^{-7}$
SrCO ₃	$5.60 \cdot 10^{-10}$
BaSO ₄	$1.08 \cdot 10^{-10}$
BaCO ₃	$2.58 \cdot 10^{-9}$
FeCO ₃	$3.13 \cdot 10^{-11}$
FeS	$8.00 \cdot 10^{-19}$
ZnCO ₃	$1.46 \cdot 10^{-10}$
ZnS(alpha)	$2.00 \cdot 10^{-25}$
ZnS(beta)	$3.00 \cdot 10^{-23}$
PbCO ₃	$7.40 \cdot 10^{-14}$
PbS	$3.00 \cdot 10^{-28}$

Table 3. Physical constants and one set of experimental parameters measured and calculated for $^{47}\text{Ca}^{2+}$ radiotracer experiments on CaCO_3 precipitation.

Parameter	Symbol	Value
Temperature	T	25 °C
Pressure	p	1.4-2.0 bar
Packed column length	Δx	60 cm
Differential pressure ^{a)}	Δp	0.4-1.0 bar
Conc. of CaCl_2	C_{CaCl_2}	5.55 g/L
Conc. of NaHCO_3	C_{NaHCO_3}	8.40 g/L
Saturation ratio ^{b)}	SR	216
Saturation index	SI	2.33
Porous material	Silica sand	106-300 μm
Porosity ^{c)}	ϕ	43.27 %
Tube cross section	A	0.2827 cm^2
Initial Darcy velocity ^{d)}	V	51 m/d
Initial volumetric flow rate	Q	0.167 cm^3/s
Permeability ^{e)}	k	6.39 darcy
Neutron flux	ϕ	$10^{13} \text{ n/cm}^2 \cdot \text{s}$
Reaction cross section	σ	$0.72 \cdot 10^{-24}$
Weight of Ca in target material	w_{Ca}	2.0 g
Atomic weight of natural Ca	M	40.078 g/mol
Abundance of ^{46}Ca in target	I_{N}	0.004 %
Gamma branch for 1297 keV	I_{γ}	84 %
Avogadro's number	N_{A}	$6.022 \cdot 10^{23}$
Half-life of ^{47}Ca	$T_{1/2, 47\text{Ca}}$	4.54 d
Irradiation time	t_i	9 d
Produced total activity ^{f)}	D_{γ}	$\sim 5 \text{ MBq}$

a) ST 3000 Smart Transmitter Differential Pressure Model (Honywell)

b) Calculated using computer model MultiScale [13]

c) Measured with the Robertson Research Helium Gas Volume Meter

d) $V = Q/A$

e) Calculated from Darcy's law: $Q = (k \cdot A \cdot \Delta p) / (\mu \cdot \Delta x)$ where μ is the viscosity of the aqueous liquids = 1 centipoise.

f) Calculated with Eqn.10.

Table 4. Nuclear data for possible radiotracers applicable for the study of scale deposition in laboratory experiments.

Element	Radio-nuclide	Tracer	Thermal (n, γ) cross section (b)	Nat. abund. target nucl. (%)	Half-life	Radiation properties: Energies in MeV, intensities in brackets in brackets
Ca	^{45}Ca	$^{45}\text{Ca}^{2+}$	^{44}Ca : 1.0	2.086	163 d	β^- : 0.258 (100), no γ
	^{47}Ca	$^{47}\text{Ca}^{2+}$	^{46}Ca : 0.72	0.004	4.54 d	β^- : 0.695 (81), 1.98 (19), γ : 1.297 (77), 0.808 (8.8), 0.489 (8.8)
Fe	^{55}Fe	$^{55}\text{Fe}^{2+}$ $^{55}\text{Fe}^{3+}$	^{54}Fe : 2.25	5.8	2.7 a	EC, no γ
	^{59}Fe	$^{59}\text{Fe}^{2+}$ $^{59}\text{Fe}^{3+}$	^{58}Fe : 1.15	0.3	45.1 d	β^- : 0.461 (54.8), 0.269 (47), γ : 1.292 (43.2), 1.099 (56.8)
Zn	^{65}Zn	$^{65}\text{Zn}^{2+}$	^{64}Zn : 0.78	48.6	244 d	β^+ : 0.32 (?), γ : 1.165 (50.75)
	$^{69\text{m}}\text{Zn}$	$^{69\text{m}}\text{Zn}^{2+}$	^{68}Zn : 0.072	18.8	13.8 h	IT γ : 0.439 (94.8)
Sr	^{85}Sr	$^{85}\text{Sr}^{2+}$	^{84}Sr : 0.81 ^{a)}	0.56	64.9 d	EC, γ : 0.514 (100)
	$^{87\text{m}}\text{Sr}$	$^{87\text{m}}\text{Sr}^{2+}$	^{86}Sr : 0.84	9.86	2.81 h	IT γ : 0.388 (82)
	^{89}Sr	$^{89}\text{Sr}^{2+}$	^{88}Sr : 0.0058	82.58	50.5 d	β^- : 1.46 (100), very weak γ
	^{131}Ba	$^{131}\text{Ba}^{2+}$	^{130}Ba : 13.5	0.106	11.5 d	EC, β^+ , γ : 0.496 (42.1), 0.124 (28), 0.216 (21.7)
Ba	$^{133\text{m}}\text{Ba}$	$^{133\text{m}}\text{Ba}^{2+}$	^{132}Ba : 0.68	0.101	38.9 h	IT γ : 0.276 (17.5)
	^{133}Ba	$^{133}\text{Ba}^{2+}$	^{132}Ba : 7.8	0.101	10.5 a	EC, γ : 0.356 (62), 0.081 (34.3), 0.303 (18.2)
	^{139}Ba	$^{139}\text{Ba}^{2+}$	^{138}Ba : 0.35	71.7	1.38 h	β^- : 2.40 (72), γ : 0.166 (22)
Pb	^{203}Pb	$^{203}\text{Pb}^{2+}$	^{203}Tl : - ^{205}Tl : -	$^{203}\text{Tl}(p,n)$: 29.5 $^{205}\text{Tl}(p,3n)$: 70.5	51.9 h	EC, γ : 0.279 (81), 0.401 (3.8)
	^{14}C	$\text{H}^{14}\text{CO}_3^-$ $^{14}\text{CO}_3^{2-}$ $^{14}\text{CO}_2$	na ^{b)}	na	5730 a	β^- : 0.159 (100)
S	^{35}S	$^{35}\text{SO}_4^{2-}$ $^{35}\text{S}^{2-}$	^{34}S : 0.240 ^{35}Cl : 75.77	4.21 $^{35}\text{Cl}(n,p)$: 0.498	87.5 d	β^- : 0.169 (100)

a) 84.5 % IT from $^{85\text{m}}\text{Sr}$ leads to this number.b) na = not applicable, i.e. ^{14}C is not foreseen produced at the authors' reactor but purchased commercially

Table 5. Calculations of activity concentration obtainable from isotopically enriched ^{46}Ca by thermal neutron irradiation with further parameters detailed in the table.

Parameter/Operation	Symbol	Value
<i>Basic parameter values:</i>		
Solubility product for CaCO_3 from Table 2	$K_{\text{sp, CaCO}_3}$	$3.36 \cdot 10^{-9}$
Applied saturation ratio	SR	1.5
Suppose symmetric conc. ^{a)} , i.e. $[\text{Ca}^{2+}] = [\text{CO}_3^{2-}]$	na	na
Approximate atomic weight of enriched Ca	M	42
Atomic weight of ^{46}Ca	$M_{46\text{Ca}}$	46
Avogadro's number	N_A	$6.022 \cdot 10^{23}$
Reaction cross section for the reaction $^{46}\text{Ca}(n_{\text{th}}, \gamma)^{47}\text{Ca}$	σ	$0.72 \cdot 10^{-24} \text{ cm}^2$
Thermal neutron flux	ϕ	$10^{13} \text{ n/cm}^2 \cdot \text{s}$
Suppose irradiation time = $1 \cdot T_{1/2}$	t_i	4.54 d
<i>Calculations:</i>		
Calculated needed conc. of Ca : $(K_{\text{sp}} \cdot \text{SR})^{1/2}$	C_{Ca}	$7.0 \cdot 10^{-5} \text{ M}$
Corresponding weight of Ca per L : $C_{\text{Ca}} \cdot M$	$w_{\text{Ca/L}}$	$2.98 \cdot 10^{-3} \text{ g/L}$
Corresponding number of ^{46}Ca atoms in 4% enriched Ca: ($4 \cdot w_{\text{Ca/L}} \cdot N_A$)/(100 $\cdot w_{\text{Ca/L}}$)	$N_{46\text{Ca}}$	$1.55 \cdot 10^{18}$ atoms/L
Activity conc. generated by irradi. in JEEP II, from Eq. 10	D	$1.11 \cdot 10^7 \text{ Bq/L}$
Gamma activity conc. with a γ -branch = 84%: $D \cdot 0.84$	D_γ	$9.36 \cdot 10^6 \text{ Bq/L}$

a) May not be true in praxis

Table 6. Estimation of how low levels of CaCO₃ precipitate that can unambiguously be detected by application of the isotopically enriched target material.

Parameters/Operations	Amount precipit., w_r , in ppm of SiO ₂ in a 1 cm long tube section			
	$w_r=1$	$w_r=10$	$w_r=1$	$w_r=10$
Solid angle viewed by collimated detector: θ (fraction) ^{a)}	0.01	0.01	0.1	0.1
Internal detector efficiency for 1297 keV γ : ϵ_i (fraction)	0.1	0.1	0.1	0.1
Calculated total detection efficiency: $\epsilon_T = \epsilon_i \cdot \theta$ (fraction)	0.001	0.001	0.01	0.01
Calculated count rate per ml of tracer solution: $R = (D_\gamma/10^3) \cdot \epsilon_T$ (cps/ml)	9.36	9.36	93.6	93.6
Liquid volume in a tube section of length $l = 1.0$ cm with porosity $\phi = 0.4$ and internal radius $r = 0.5$ cm: $V_l = \pi \cdot r^2 \cdot l \cdot \phi$ (ml)	0.314	0.314	0.314	0.314
Count rate of liquid volume V_l : $R_V = R \cdot V_l$ (cps)	2.94	2.94	29.4	29.4
Mass of packing material SiO ₂ in the same tube section when solid volume fraction = $1-\phi$ and density of SiO ₂ is $\rho_{SiO_2} = 2.65$ g/cm ³ : $w_{SiO_2} = \pi \cdot r^2 \cdot l \cdot (1-\phi) \cdot \rho_{SiO_2}$ (g)	1.25	1.25	1.25	1.25
Mass of Ca in precipitate corresponding to w_r : $w_p = (w_{SiO_2} \cdot w_r / 10^6) \cdot (M_{Ca} / M_{CaCO_3})$ (g)	$5.15 \cdot 10^{-7}$	$5.15 \cdot 10^{-6}$	$5.15 \cdot 10^{-7}$	$5.15 \cdot 10^{-6}$
γ disintegration rate of precipitate corresponding to various w_r -values: $D_{\gamma,p} = (D_\gamma \cdot w_p) / w_{Ca,L}$ (Bq)	$1.62 \cdot 10^3$	$1.62 \cdot 10^4$	$1.62 \cdot 10^3$	$1.62 \cdot 10^4$
γ count rate of precipitate corresponding to various w_r -values: $R_p = D_{\gamma,p} \cdot \epsilon_T$ (cps)	1.62	16.2	16.2	162
Selected counting time t_c (s)	60	60	60	60
Total number of counts in the counting time: $S_T = (R_V + R_p) \cdot t_c$ (cpm) ^{b)}	274 ± 17	1148 ± 34	2736 ± 52	11484 ± 107
Net number of counts from CaCO₃ precipitate only: $S_N = R_p \cdot t_c$ (cpm) ^{b)}	97 ± 19	972 ± 46	972 ± 61	9720 ± 146

\Downarrow \Downarrow \Downarrow \Downarrow

1 ppm detected $\sigma_{rel} = 20\%$	10 ppm well detected $\sigma_{rel} = 5\%$	1 ppm well detected $\sigma_{rel} = 6\%$	10 ppm very well detected $\sigma_{rel} = 1.5\%$
---	--	---	---

- a) The selection of a narrow collimation covering a solid angle of 1% and a wide collimation covering a solid angle of 10 % are arbitrarily chosen but realistic.
- b) The errors given represent an uncertainty in the counting numbers only of 1 standard deviation.

Fig.1

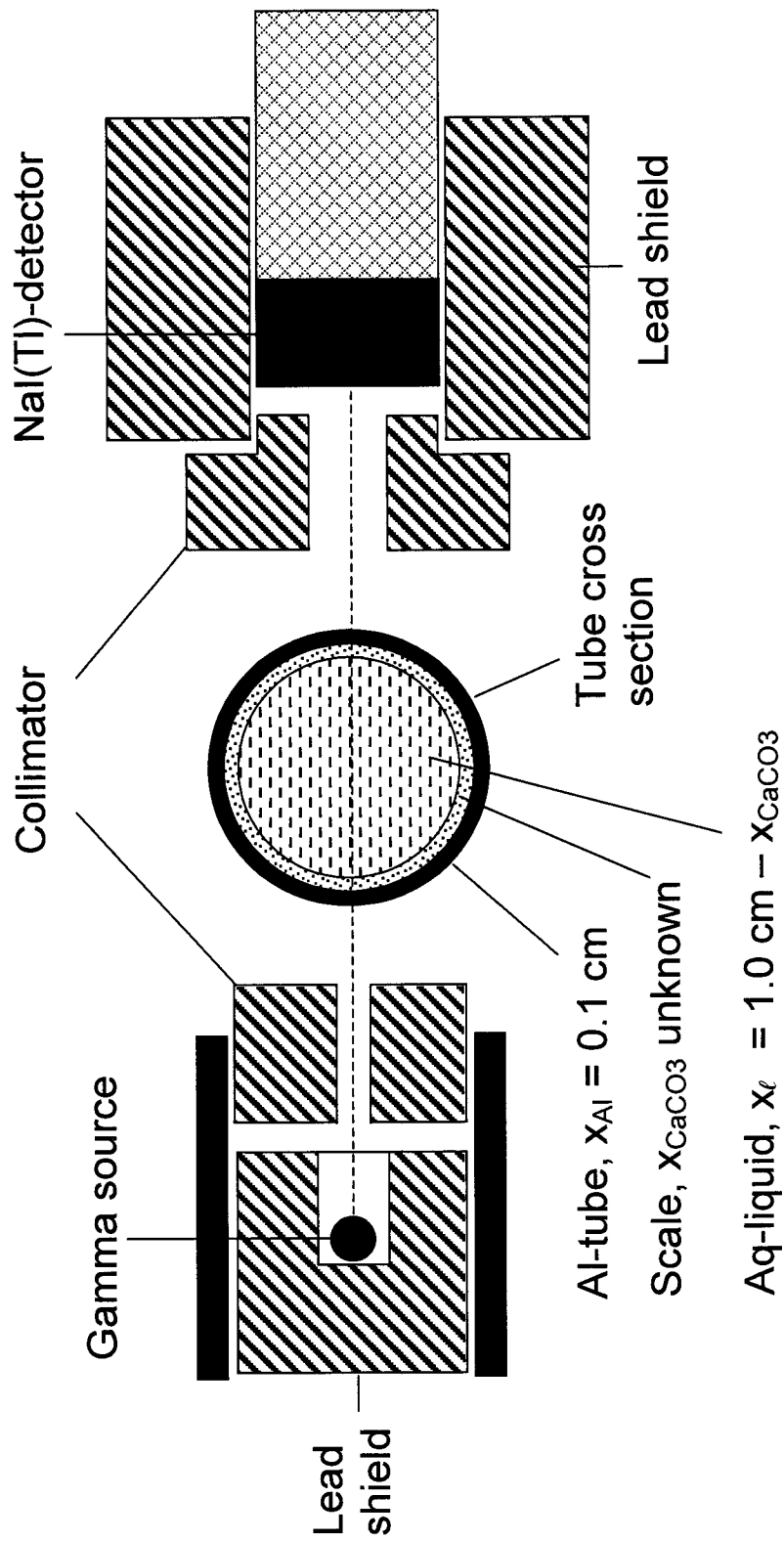


Fig.2

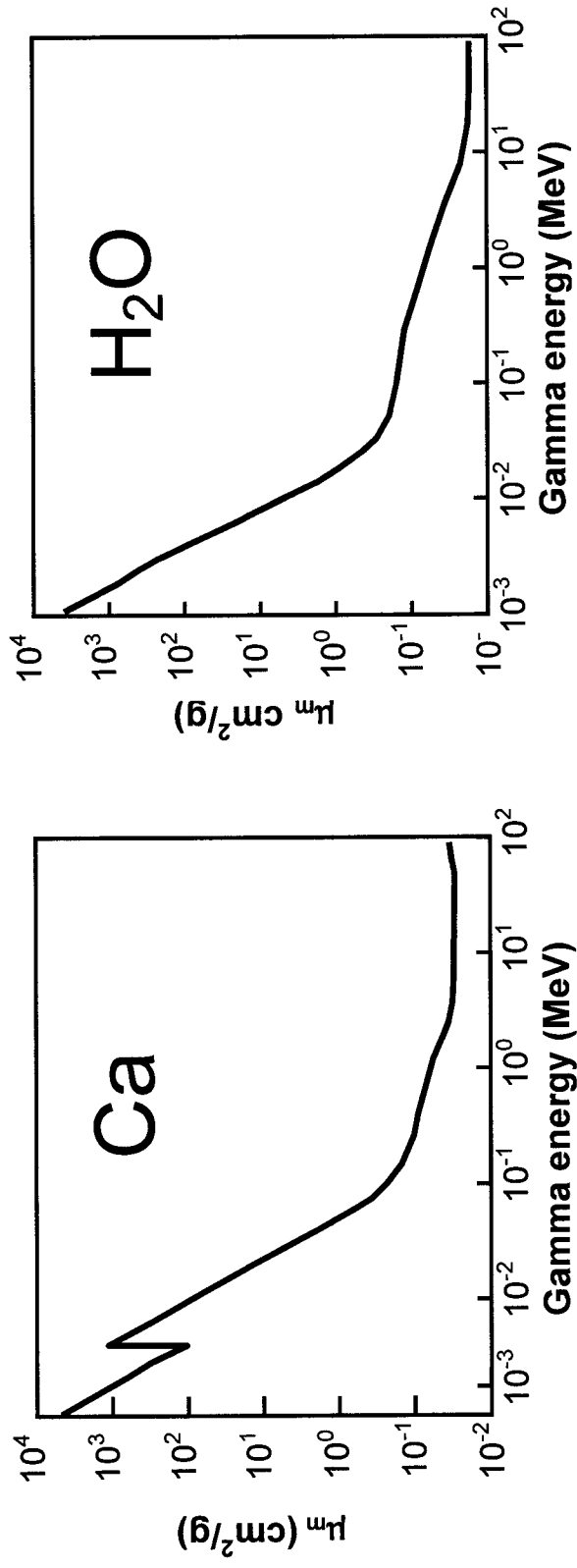
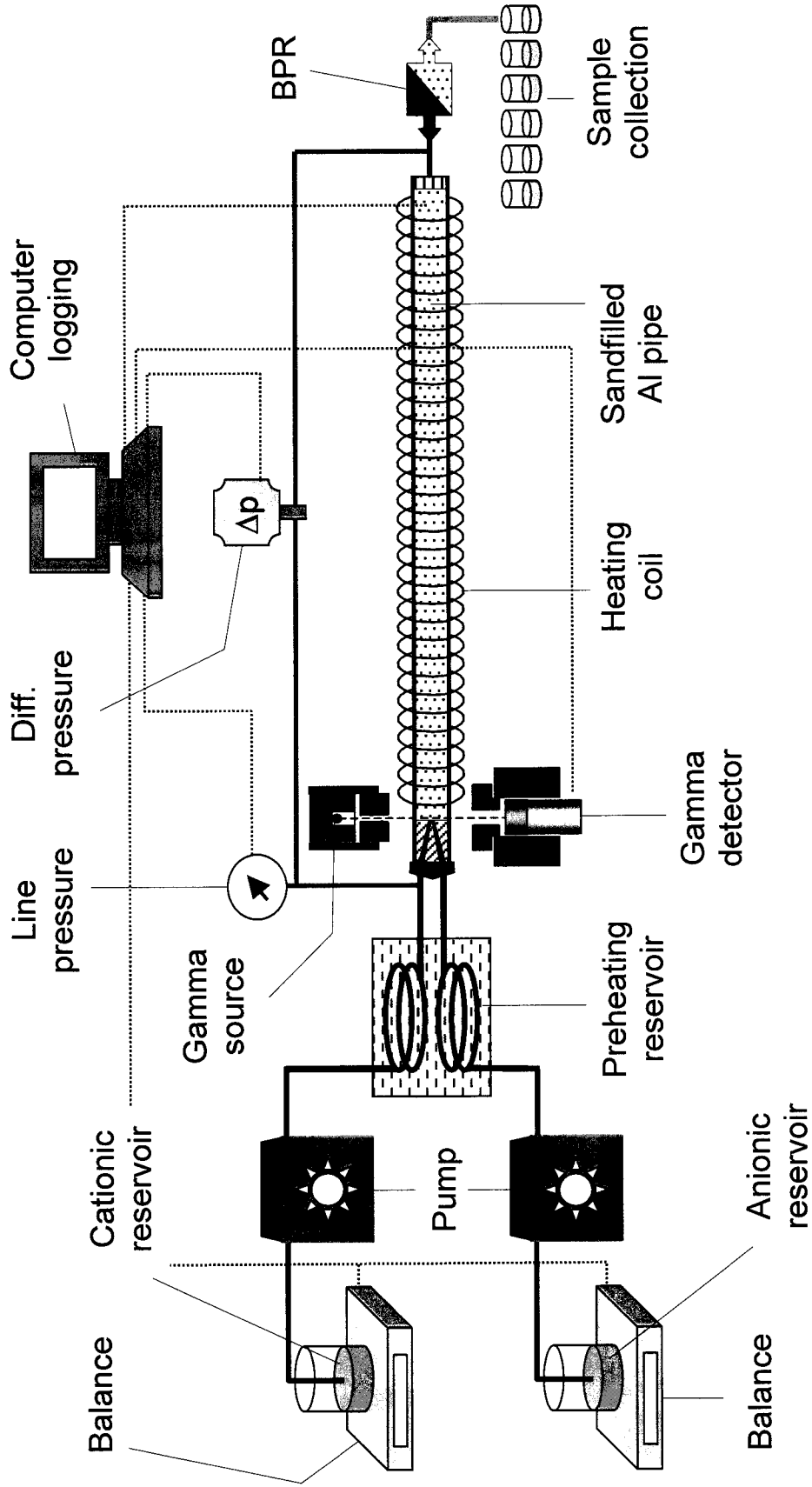


Fig.3



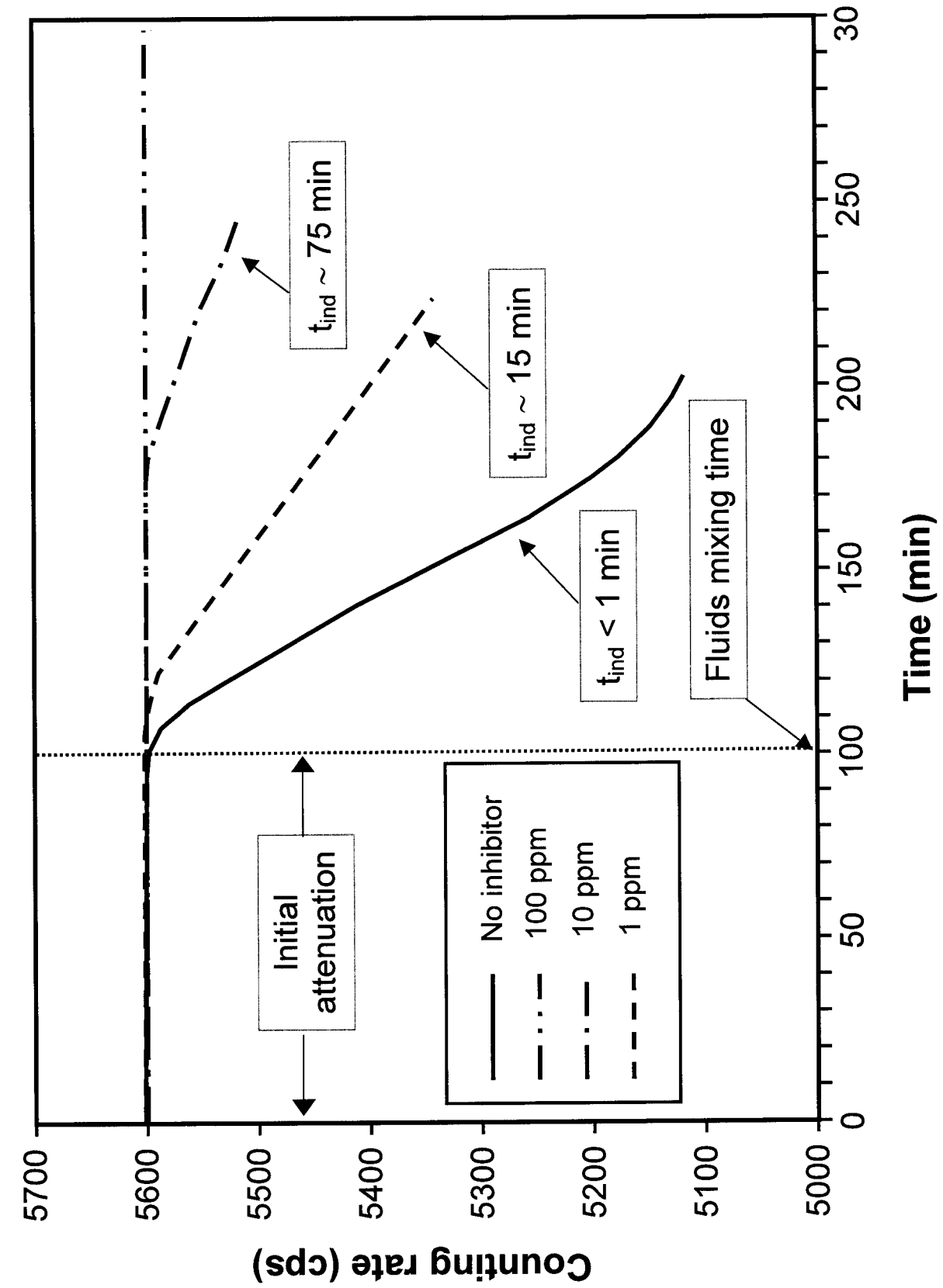


Fig.4.

Fig.5

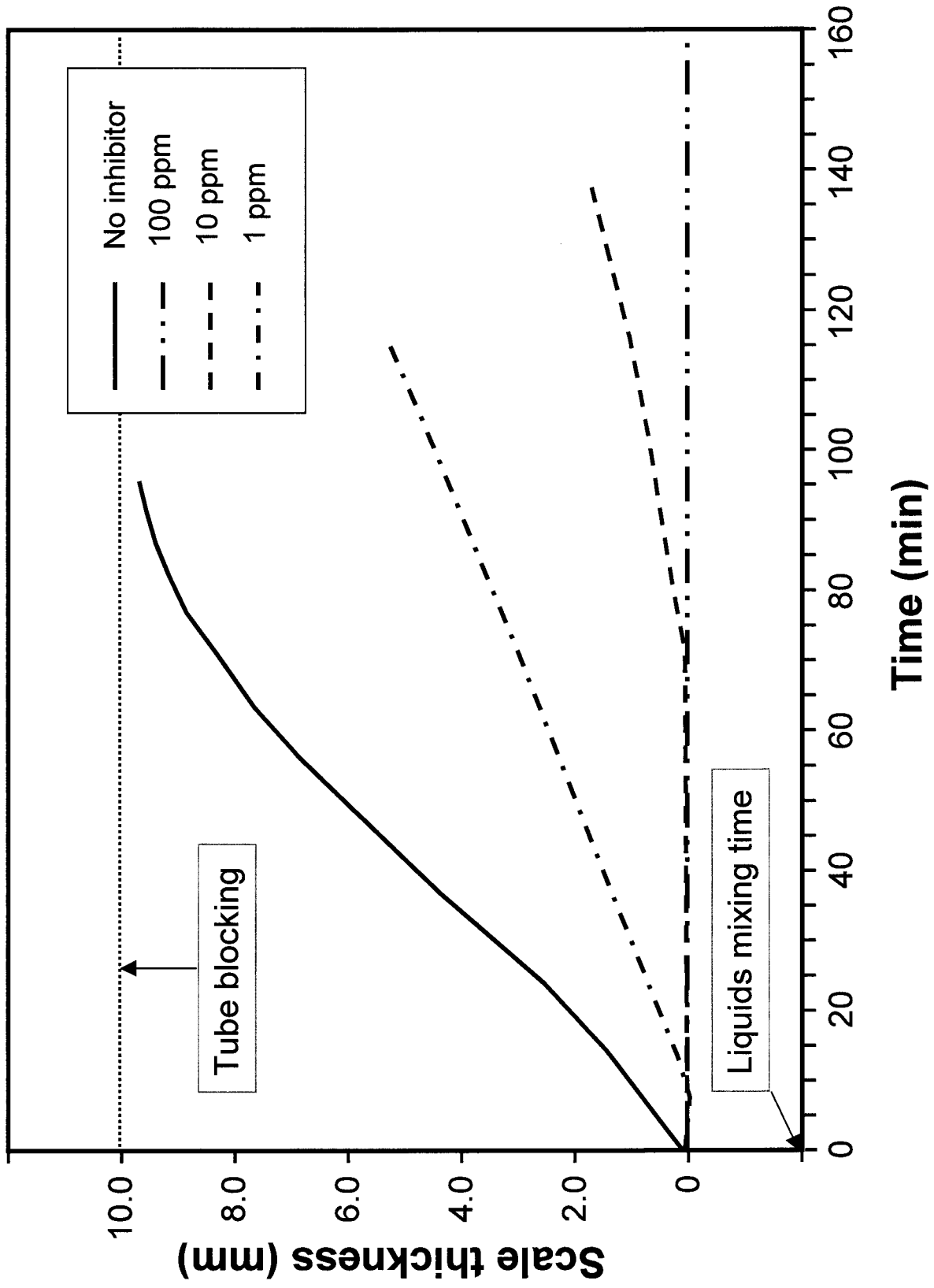


Fig.6

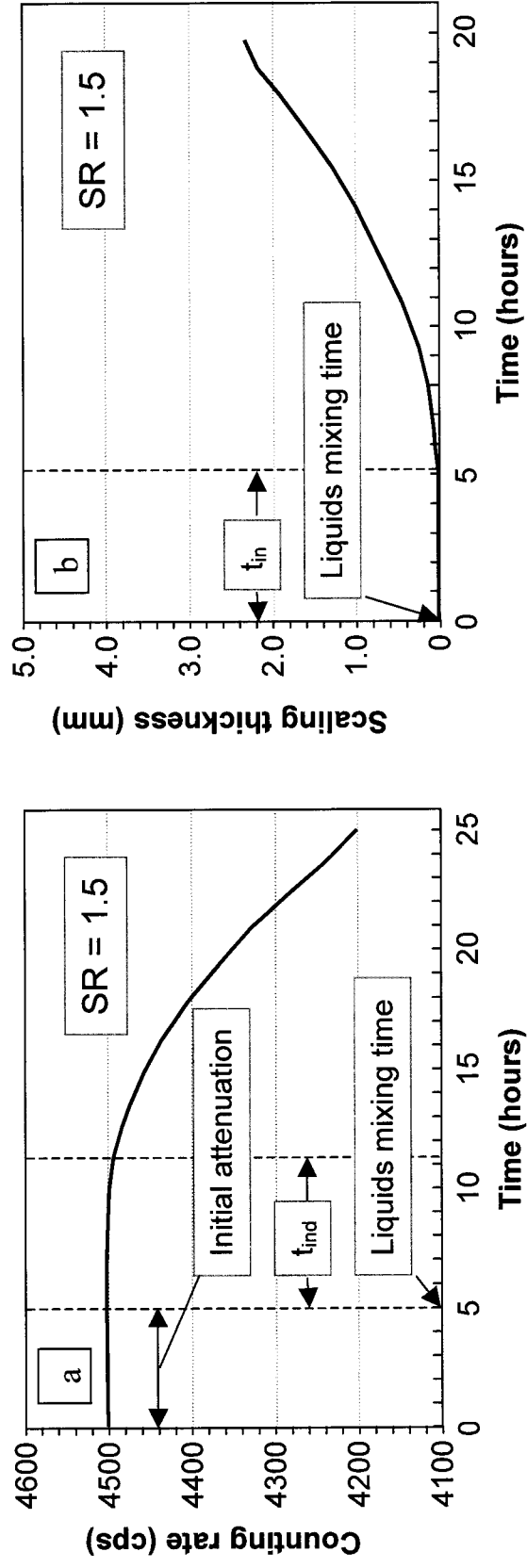


Fig.7

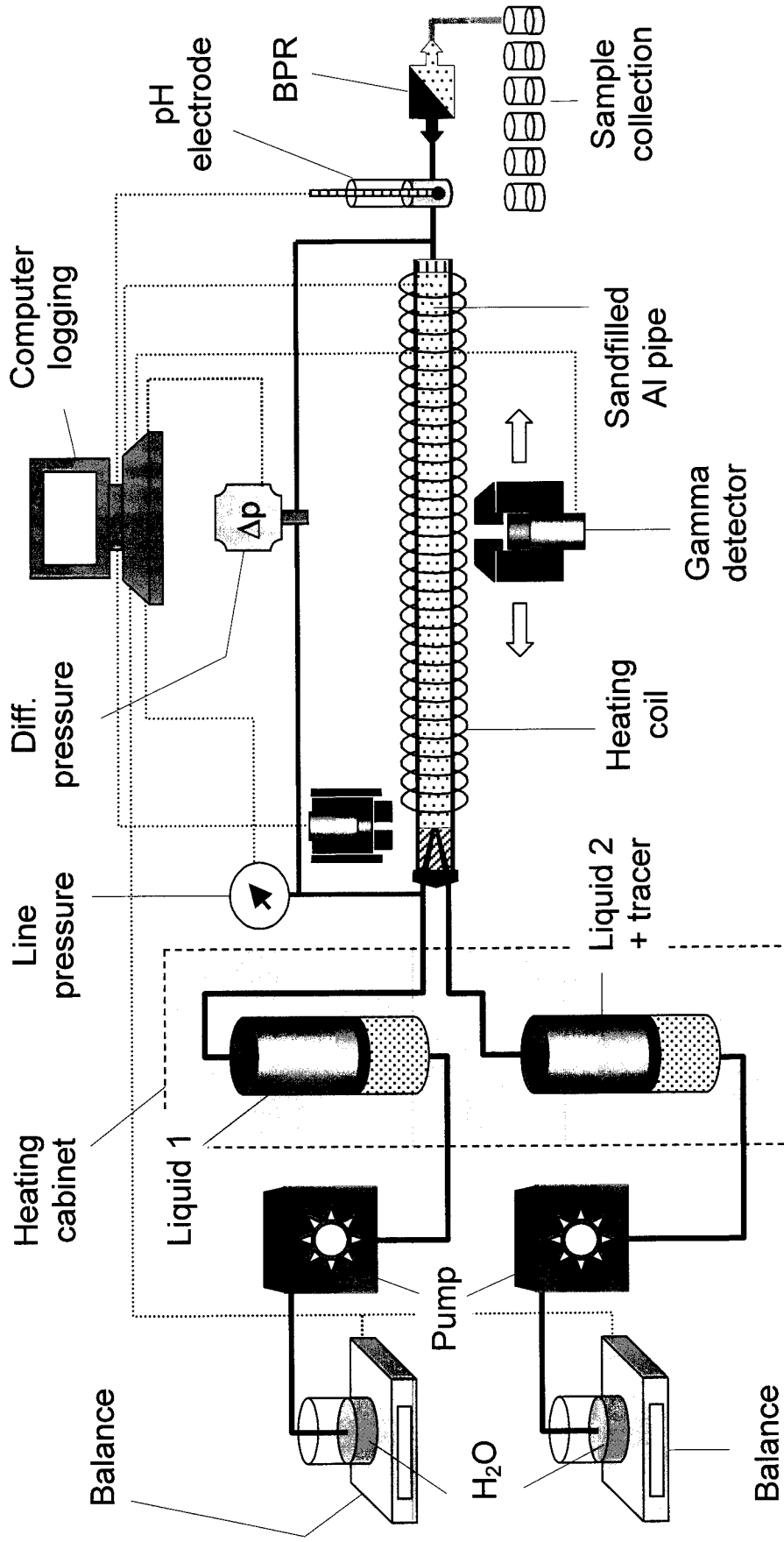


Fig.8

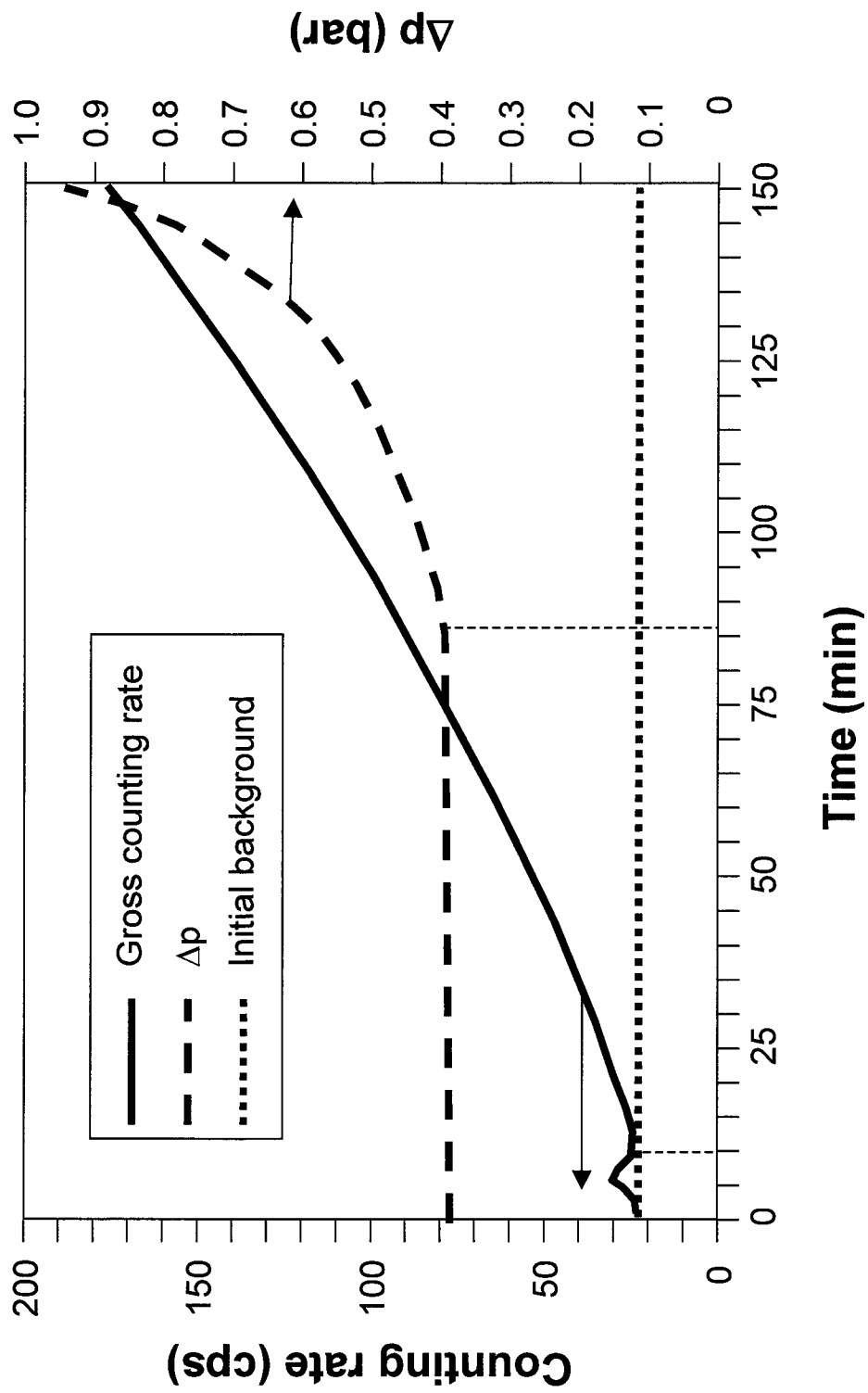


Fig.9

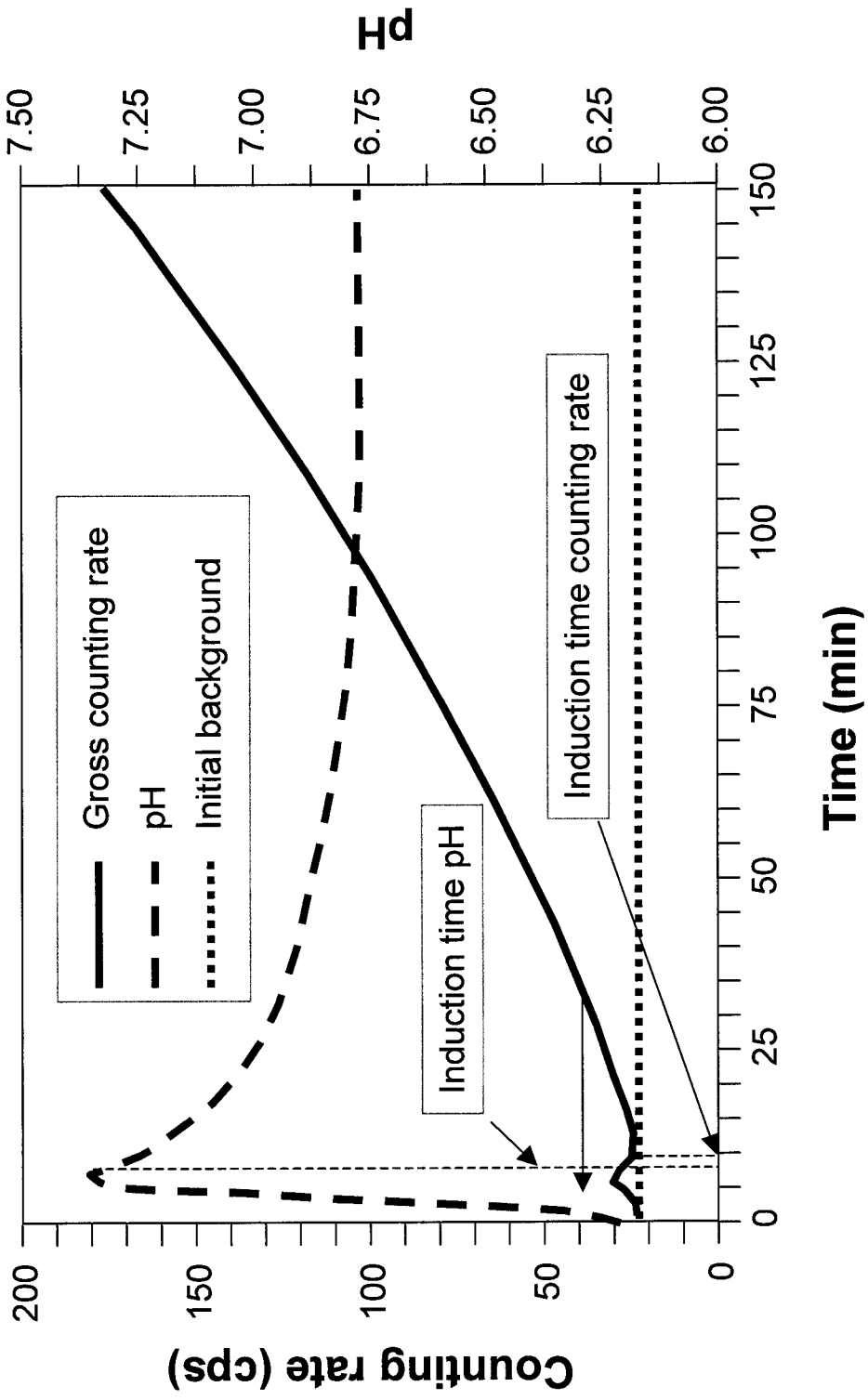


Fig.10

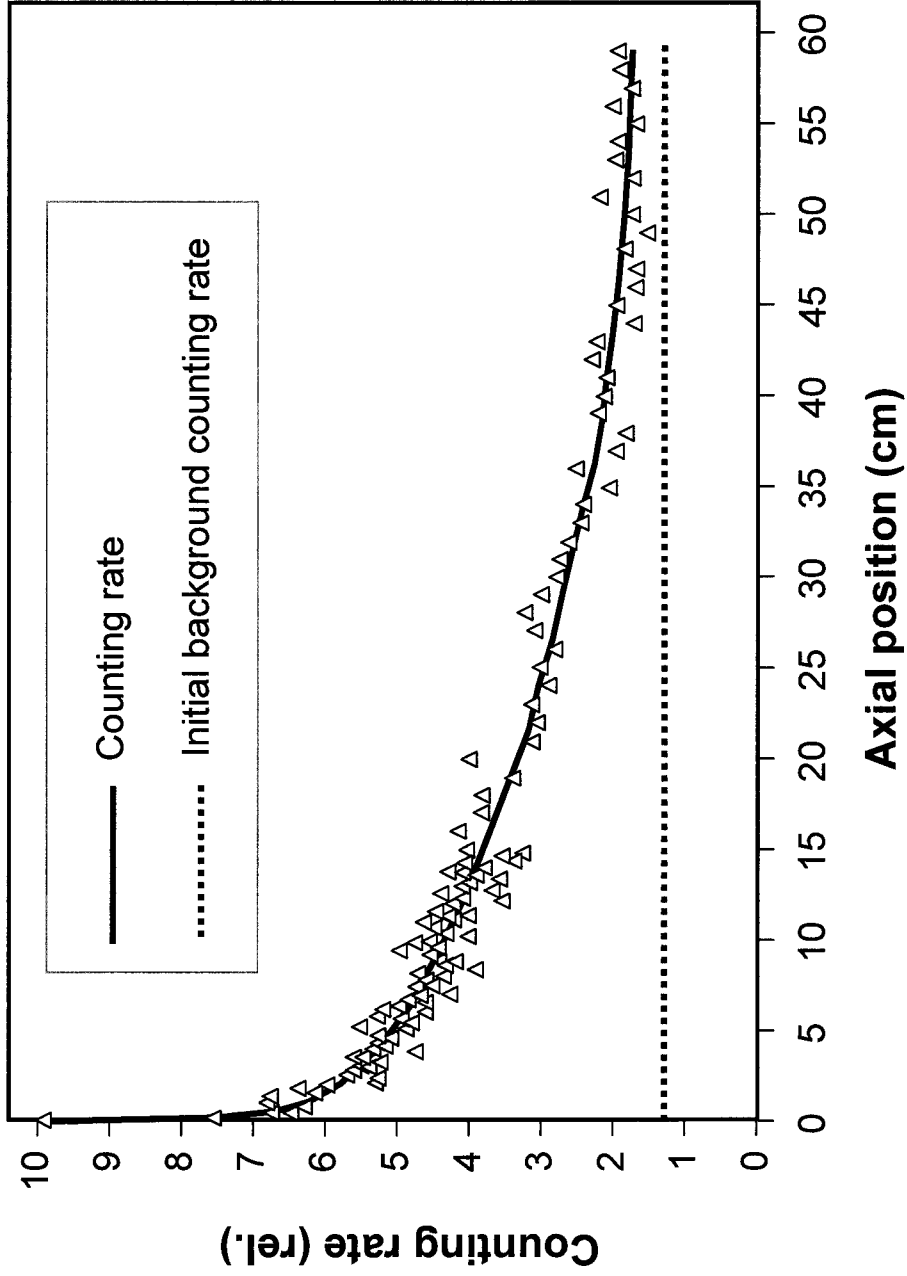


Fig.11

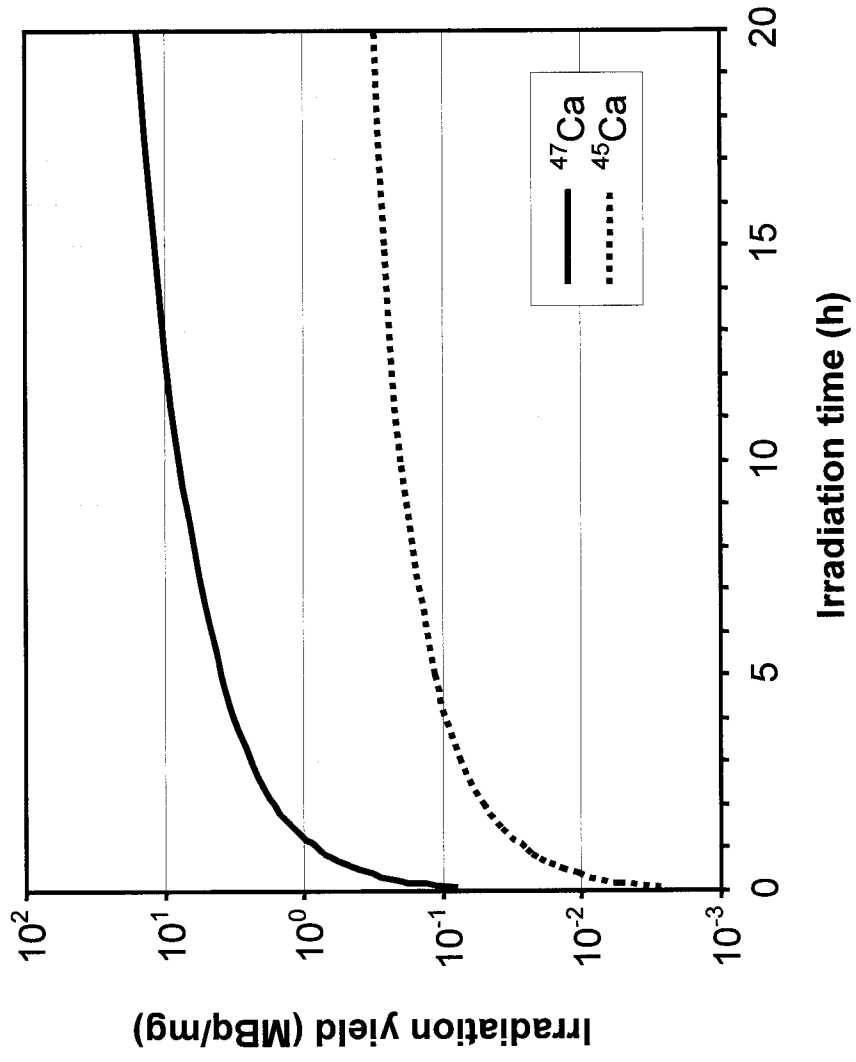


Fig.12

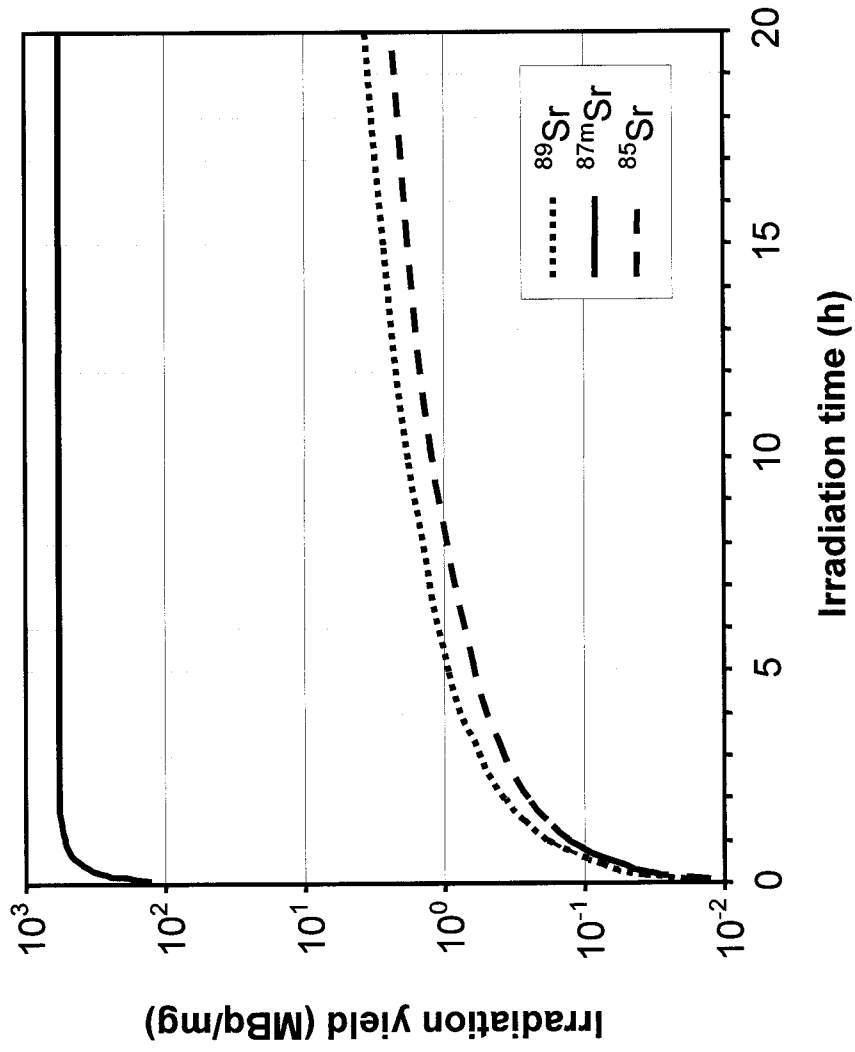


Fig.13

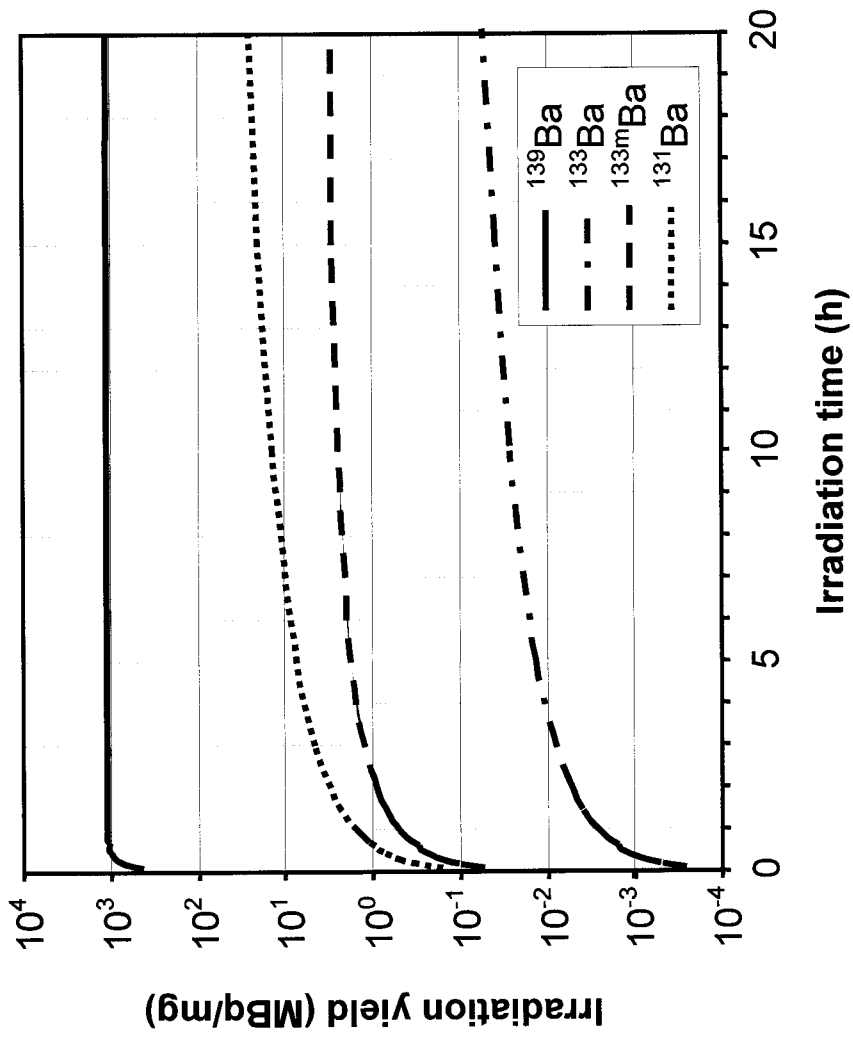


Fig.14

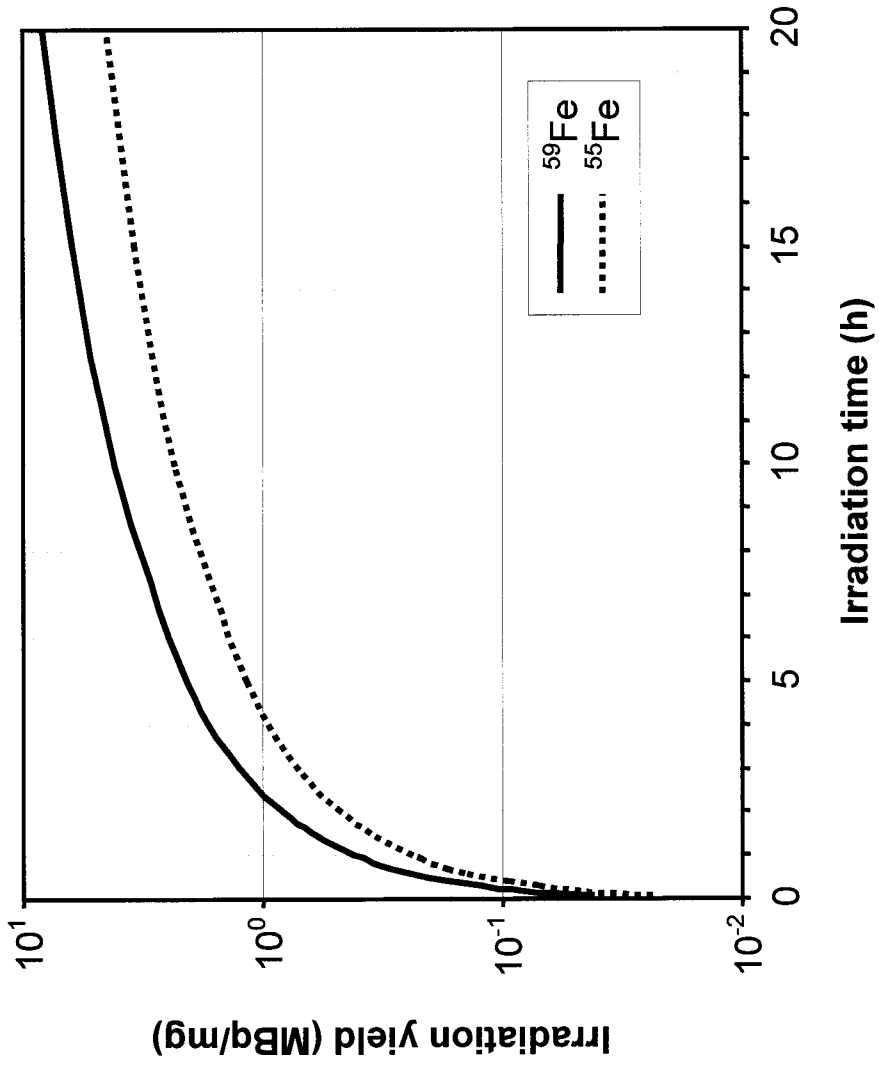


Fig.15

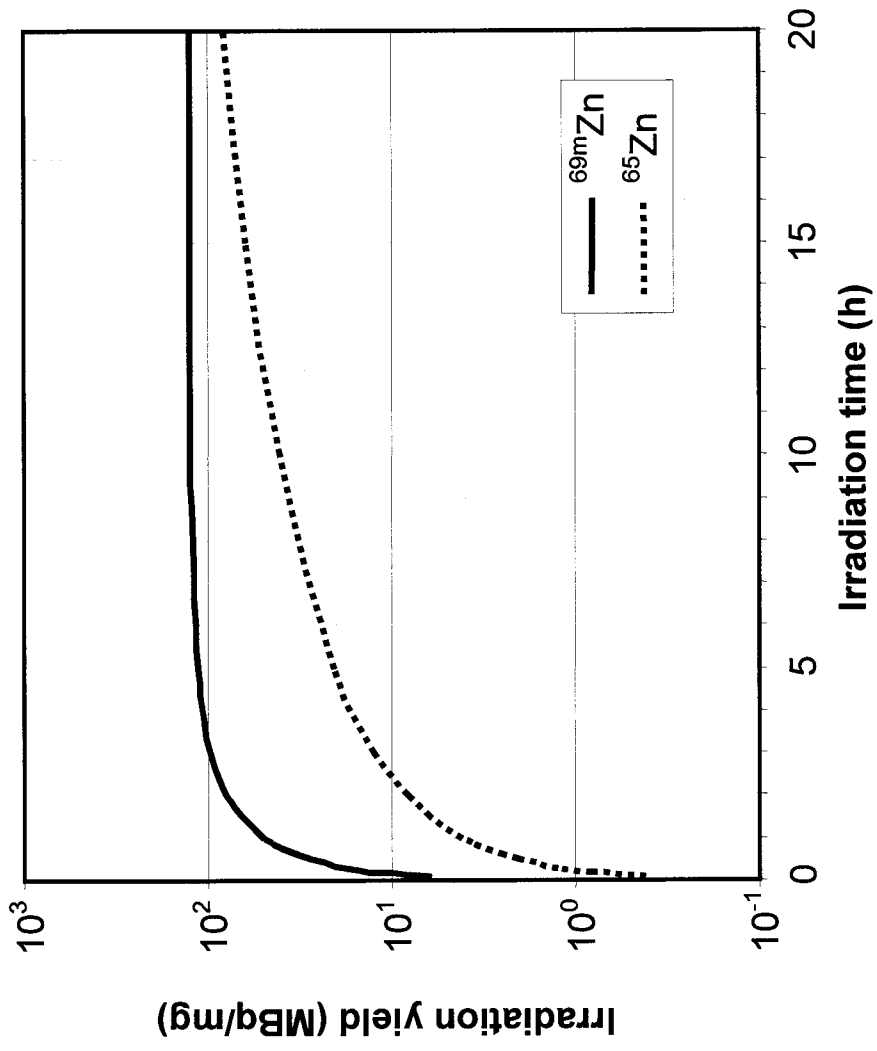


Fig. 1. Principle sketch of the gamma transmission method showing the source and detector geometry relative to the non-packed tube where scaling takes place on the inner walls.

Fig 2. Examples of mass absorption coefficients for components involved in gamma transmission measurements of the scaling process (reproduced from [12]).

Fig.3. Sketch of the experimental setup for the gamma transmission measurements. The tube can be scanned across the fixed and stationary source-detector arrangement at intervals.

Fig.4. Gamma attenuation measurements on calcite precipitation in a non-packed flooding tube at a saturation ratio of $SR = 20$ in the absence and presence of scale inhibitor Na_2AMP with detector in a fixed position 10 cm from the mixing point in the reaction tube at 185 °C. The curves are fits to the original scatter plots.

Fig.5. Scaling rate (scale thickness as a function of time) of $CaCO_3$ precipitation in the absence and presence of scale inhibitor. The data is converted from Fig.4 by the use of Eqn.9. The curves are fits to the original scatter plots.

Fig.6. a. Gamma attenuation measurements of calcite precipitation at the inlet of the non-packed flow tube (first 0.5 cm) at 160 °C, 15 bars and $SR = 1.5$. b. Scaling rates (scale thickness as a function of time) of calcite precipitation at the inlet of the tube (first 0.5 cm) converted from the primary data in Fig.6a. The curves are fits to the original scatter plots.

Fig.7. Sketch of the experimental setup for the tracer measurements. The flow tube, which is filled with silicate sand SiO_2 , is mounted in a fixed position, and the collimated detector may be scanned along the tube axis.

Fig.8. Deposition of ^{47}Ca (proportional to the deposition of $CaCO_3$) at position 0 (liquid mixing point at the inlet of the tube) as a function of time and the corresponding build-

up of differential pressure over the entire sand pack. Experimental details are found in Table 3. The curves are fits to the original scatter plots.

Fig.9. Similar to Fig.8, deposition of ^{47}Ca as a function of time compared to the corresponding development in recorded pH at the exit of the tube. Experimental details are found in Table 3. The curves are fits to the original scatter plots.

Fig.10. Total counting rate of ^{47}Ca along the flow tube axis recorded with the gamma scanner at the end of the experiment. When corrected for liquid background and after proper calibration, this curve represents the mass of deposited CaCO_3 as a function of position in the sand pack

Fig.11. Irradiation yields in MBq/mg natural elemental composition as a function of irradiation time for applicable radioactive calcium isotopes. Thermal flux is $10^{13} \text{ n}\cdot\text{cm}^{-2}\cdot\text{s}^{-1}$. Further experimental parameters are given in Table 4.

Fig.12. Irradiation yields in MBq/mg natural elemental composition as a function of irradiation time for applicable radioactive strontium isotopes. Thermal flux is $10^{13} \text{ n}\cdot\text{cm}^{-2}\cdot\text{s}^{-1}$. Further experimental parameters are given in Table 4.

Fig.13. Irradiation yields in MBq/mg natural elemental composition as a function of irradiation time for applicable radioactive barium isotopes. Thermal flux is $10^{13} \text{ n}\cdot\text{cm}^{-2}\cdot\text{s}^{-1}$. Further experimental parameters are given in Table 4.

Fig.14. Irradiation yields in MBq/mg natural elemental composition as a function of irradiation time for applicable radioactive iron isotopes. Thermal flux is $10^{13} \text{ n}\cdot\text{cm}^{-2}\cdot\text{s}^{-1}$. Further experimental parameters are given in Table 4.

Fig.15. Irradiation yields in MBq/mg natural elemental composition as a function of irradiation time for applicable radioactive zinc isotopes. Thermal flux is $10^{13} \text{ n}\cdot\text{cm}^{-2}\cdot\text{s}^{-1}$. Further experimental parameters are given in Table 4.

